Evaluation of Permanent Magnet Effects on the Performance of PMa-SynRM in Electric Vehicles

Zhenghao Liu[1], Shuhui Li[2], Yang-Ki Hong[3], Sayem Ul Alam[4]
Department of Electrical and Computer Engineering
The University of Alabama
Tuscaloosa, Alabama 35487, USA
[1]zliu99@crimson.ua.edu, [2]sli@eng.ua.edu, [3]ykhong@eng.ua.edu, [4]salam7@crimson.ua.edu

Abstract **—Permanent-magnet-assisted synchronous reluctance motors (PMa-SynRMs) show strong potential for EV propulsion, yet the impact of different PM B–H characteristics on their performance remains insufficiently understood. This paper evaluates four commercial PM types—sintered NdFeB, SmCo, bonded NdFeB, and ferrite—using identical machine geometry, winding, and inverter limits in ANSYS Motor-CAD. Comparative tests against a pure SynRM across multiple DC-link voltages and current levels examine torque, power, power factor, and efficiency. Results show that ferrite provides meaningful performance gains at low cost, while NdFeB delivers the highest torque (368.9 Nm), power (345.3 kW), and efficiency (>92%). Overall, the comparison highlights the trade-offs between magnetic strength, temperature stability, and economic feasibility, providing useful insights for optimizing PMa-SynRM to approach IPM-level performance across various vehicle voltage and current levels.**

Index Terms—synchronous reluctance (SynRM), permanent magnet assisted synchronous reluctance (PMa-SynRM), back-electromotive force (back-EMF), intrinsic coercivity, power factor.

I. Introduction

Permanent-magnet synchronous machines (PMSMs) are widely used in transportation electrification—such as battery electric vehicles (EVs), and electric aircraft—because of their high torque density, excellent efficiency, and broad speed range achieved through mature vector-control and field-weakening techniques [1]–[3]. Most PMSMs use NdFeB or other rare-earth permanent magnets (PMs), whose cost and availability depend on a limited global supply chain and energy intensive extraction and refining processes. With the rapid increase in EV production, the demand for rare-earth magnet materials has surged, exposing the motor industry to price volatility and supply risk, and environmental concerns [4], [5].

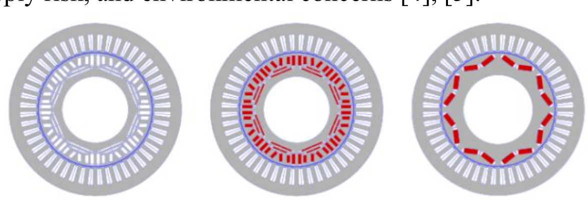

Fig.1. Illustration of (a) a synchronous reluctance, (b) a permanent magnet assisted synchronous reluctance, and (c) an interior permanent magnet motor.

In response to these challenges, PMa-SynRMs (Fig. 1b) have become a promising design option. By embedding a relatively modest amount of PM within saliency-optimized flux barriers, the PMa-SynRM combines the reluctance-torque advantages of a SynRM (Fig. 1a) with the flux-enhancement of PMs. This topology thus enhances torque density, power factor, and field-weakening capability compared to a SynRM. Recent studies show that an optimized PMa-SynRM can approach the performance of an IPM (Fig. 1c) for traction applications while using significantly less rare-earth PM [6], [7].

In a PMa-SynRM, PMs play a crucial role in determining overall performance. However, different PM materials exhibit distinct magnetic characteristics, such as variations in the B–H curve and maximum energy product (BH_{max}). The extent to which these differences influence PMa-SynRM performance remains unclear. Therefore, this paper presents an assessment and comparative study on the impact of various PM materials on PMa-SynRM performance, with a particular focus on EV applications. Four delegate commercial rare-earth magnets are examined in this analysis, including sintered NdFeB (e.g., N35UH), SmCo (e.g., Recoma 28), bonded NdFeB (e.g., MQP series), and hard ferrite (e.g., Y32). All cases maintain the same stator geometry, rotor flux barrier layout, winding, and inverter current limits in a single design framework implemented in ANSYS Motor-CAD.

While previous research has examined the performance of PMa-SynRM using specific magnet materials or geometry-optimized designs, this study presents a comparative FEM analysis that is invariant to geometry, focusing solely on the effects of permanent-magnet material properties. To the best of the authors' knowledge, this study is among the first to systematically evaluate multiple permanent-magnet classes for PMa-SynRM machines. This controlled framework provides valuable insights into magnet material selection at the design level, extending beyond mere peak-performance evaluations and offering practical recommendations for optimizing EV traction motors within the constraints of real inverters.

II. PMa-SynRM: Models and Operation Constraints

A. PMa-SynRM Models

The PMa-SynRM combines the advantages of both PM excitation and synchronous reluctance torque. By embedding PMs in a motor rotor, the motor generates additional torque from the interaction between motor stator currents and rotor PM

979-8-3315-8138-1

flux, while the rotor saliency produces reluctance torque. The compared equivalent phasor diagrams of a SynRM and a PMa-SynRM are shown on Fig. 2.

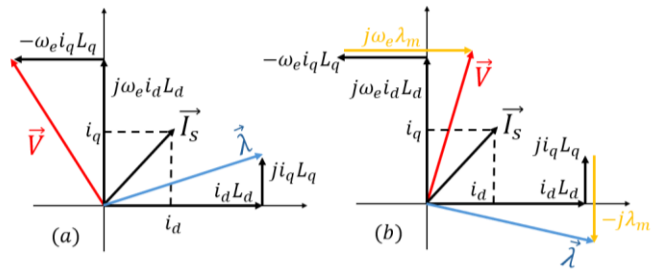

Fig. 2. Electrical phasor diagram of (a) SynRM and (b) PMa-SynRM motor.

The PMa-SynRM exhibits a significant difference in the total flux linkage compared with the pure SynRM, primarily due to the additional magnet flux component, λ_m. The flux linkages of the motors can be written as

$$\lambda_d(i_d, i_q) = L_d(i_d, i_q)i_d + \lambda_m(i_q) \quad (1)$$

$$\lambda_q(i_d, i_q) = L_q(i_d, i_q)i_q, \quad (2)$$

where can the motor still generate torque even when $i_d = 0$ based on λ_m as

$$\lambda_m(i_q) = \lambda_d(i_d = 0, i_q \neq 0) \quad (3)$$

The electrical equations of a PMa-SynRM include motor's stator d- and q-axis equations as

$$v_d = R_s i_d - \omega L_q i_q + \frac{d\lambda_d}{dt} \quad (4)$$

$$v_q = R_s i_q + \omega L_d i_d + \omega \lambda_m + \frac{d\lambda_q}{dt} \quad (5)$$

The torque model of a PMa-SynRM is

$$T = \frac{3}{2}p[(\lambda_d + \lambda_m)i_q - \lambda_q i_d] \quad (6)$$

To evaluate the performance of PMa-SynRM, the power factor is the key performance indicator that describes how effectively the motor converts input electrical power into useful mechanical power. It reflects the phase relationship between the stator current and the stator voltage. The input power of the motor is

$$P = \frac{3}{2}(V_d I_d + V_q I_q) \quad (7)$$

Hence, the power factor can be numerically derived from:

$$PF = \frac{P}{\sqrt{P^2+Q^2}} \quad (8)$$

where $Q = \frac{3}{2}(V_q I_d + V_d I_q)$ is the reactive power.

B. PMa-SynRM operation constraints

In the PMa-SynRM, the operating point in the *d-q* frame is bounded by the current limit, I_s, and the speed-dependent voltage limit, V_{s_max}. At low speed, only the current circle is active, and the controller follows the Maximum Torque per Ampere (MTPA) trajectory in (9) for a maximum torque output.

$$I_s = \sqrt{i_d^2 + i_q^2} \leq I_{s\_max} \quad (9)$$

As speed increases, the voltage ellipse shrinks, requiring additional negative i_d for flux weakening (FW) to keep the operating point inside both limits. At high speed, both constraints become active at the same time, and the machine operates in the Maximum Torque per Voltage (MTPV) region, where i_d and i_q are tuned to extract the highest feasible torque along the intersection of the current and voltage boundaries alone in (10).

$$V_{s\_max} = p\sqrt{(L_d i_d + \lambda_m)^2 + (L_q i_q)^2} \leq \frac{V_{dc}}{\sqrt{3}\omega_e} \quad (10)$$

The formulations presented above adhere to the conventional PMa-SynRM modeling techniques that are extensively documented in existing literature. They are included in this study to outline the operational constraints and evaluation framework utilized. This study does not introduce any novel theoretical motor models; rather, it emphasizes the impact of magnet material characteristics on operating trajectories and performance boundaries.

III. PMA-SYNRM DESIGN

A PMa-SynRM typically combines the high-efficiency torque production of a SynRM with the improved flux capability offered by strategically placed PMs. The magnets do not provide full excitation as in a PMSM; instead, they assist the reluctance torque by enhancing the air-gap flux, increasing saliency, improving torque density, and reducing torque ripple. This dual-torque mechanism intends to enable higher efficiency, better power factors, and improved performance over pure SynRMs, while using significantly fewer magnets than traditional PMSMs.

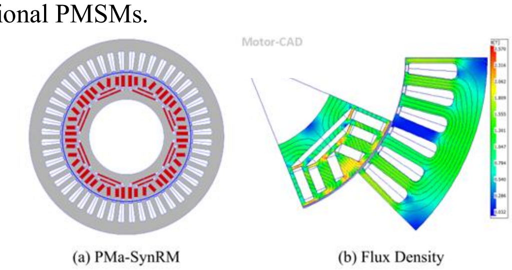

Fig. 3. (a) An illustration of an 8-pole, 4-flux-layer PMa-SynRM and (b) the magnetic flux density of Nd-Fe-B (N35UH).

A standard design of PMa-SynRM is developed in this study as shown in Fig. 3(a). The machine maintains the salient-pole topology of a conventional SynRM but includes embedded PMs (red in Fig. 3a) within the rotor flux barriers. The magnets are placed along the middle of each barrier to align the magnetic flux with the *d*-axis and enhance the air-gap flux linkage. The rotor is designed with four flux-barrier layers per pole to balance mechanical strength, magnetic saliency, and resistance to demagnetization. The stator features a distributed three-phase winding in a 48-slot layout.

Fig. 3(b) shows the magnetic flux density distribution of the designed PMa-SynRM with NdFeB magnets as an example. The contour plot clearly illustrates a flux path connecting the rotor barriers and stator teeth, highlighting strong magnet excitation and the effective use of both PM and reluctance flux components. The flux is well distributed across the rotor barriers, with only minor local saturation around the bridge

979-8-3315-8138-1

areas, confirming that the rotor geometry maintains strong mechanical strength without sacrificing magnetic performance. Overall, the flux pattern confirms that the embedded NdFeB magnets effectively reinforce the d-axis flux linkage, enhancing both torque density and power factor in the PMa-SynRM design [9].

All material and geometric parameters were modeled and optimized in ANSYS Motor-CAD to ensure consistent electromagnetic loading across different magnet types. This setup serves as the baseline for comparing how different magnets, including NdFeB, SmCo, bonded NdFeB, and ferrite, affect torque production and efficiency. Based on the PMa-SynRM design shown in Fig. 3, we will replace NdFeB (N35UH) magnet with three other PMs during motor performance evaluation in the following sections.

IV. Magnetic Property Comparison

The four permanent-magnet materials selected in this study represent commercial and technical options for EV traction motors. Sintered NdFeB is highlighted in the performance due to its high remanence and energy density, while SmCo is included for its excellent thermal stability and demagnetization resistance. Bonded NdFeB offers reduced iron losses and flexible manufacturability at the weakened magnetic strength. The ferrite provides a low-cost, rare-earth-free alternative. Together, these materials enable a balanced solution of performance and cost trade-offs in EV applications.

To evaluate how PM properties affect PMa-SynRM performance, four commercial PMs are selected. Their magnetic parameters and cost are shown in Table I and major magnetic characteristics are further accessed in this section.

TABLE I. Magnetic Parameters and Cost Comparison for Assessed PM.

Magnet Type	B_r (T)	H_c (kA/m)	$H_{c,j}$ (kA/m)	$(BH)_{max}$ $(MGOe)$	Relative Cost
NdFeB (N35UH)	1.21	917	1990	36	5
SmCo (Recoma 28)	1.1	826	2000	28	8
Bonded NdFeB (MQP-12-8HD)	0.78	475	645	13	3
Ferrite (Y32)	0.41	167	180	4	1(lowest)

A. Summary Evaluation of Permanent Magnets

Sintered Nd-Fe-B (N35UH) magnet exhibits the highest maximum energy product $(BH)_{max}$. However, it has a low Curie temperature of 523 K, which can lead to thermal instability, and it is also a rare-earth magnet that is corrosive. In contrast, the bonded Nd-Fe-B (MQP-12-8HD) magnet is magnetically isotropic and resistant to corrosion, but its $(BH)_{max}$ is much lower than that of the sintered NdFeB (N35UH). Its advantages include flexibility in manufacturing and reduced eddy-current loss. The expensive, high-Curie-temperature (around 900 K) SmCo (Recoma 28) is highly resistant to corrosion and is therefore utilized in aerospace and precision machinery applications. Its $(BH)_{max}$ is slightly lower than that of sintered Nd-Fe-B. Ferrite (Y32) is a rare-earth-free PM that is highly cost-effective. Its $(BH)_{max}$ is significantly lower compared to Nd-Fe-B and SmCo, but it offers excellent corrosion resistance because of its oxide form. An advantage of ferrite magnets is their increased coercivity at higher temperatures. Therefore, ferrite magnets are used in PMa-SynRM design [10-13].

B. Demagnetization Characteristic Evaluation

Demagnetization is not only a loss of magnetic strength but also a torque production issue. Once the magnet's flux density is irreversibly reduced beyond its knee point, the machine's air-gap flux density permanently decreases, resulting in lower torque and efficiency. Unlike resistive losses or thermal decreasing, this effect is irreversible even when current or temperature is simply lowered; the magnet is deeply altered.

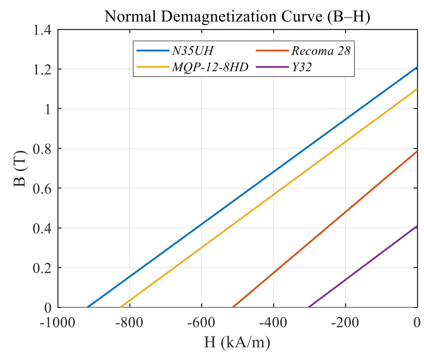

Fig. 4. Comparison of four normal demagnetization curves at room temperature for Nd-Fe-B, SmCo, bonded Nd-Fe-B, and ferrite on Table I.

The normal demagnetization curves are shown in Fig. 4 for the four selected PMs in Table I. As shown in Fig. 4, Nd-Fe-B exhibits the highest remanent flux density (B_r), indicating a greater maximum energy density ($(BH)_{max}$). SmCo has slightly lower B_r and $H_{c,j}$, showing nearly the same magnetic stability at room temperature as sintered Nd-Fe-B.

C. Remanent and Coercivity of Permanent Magnets

Magnets with high remanent flux density enhance torque density and reduce current demand at low speeds. Still, they require higher coercivity to safely withstand the significant negative i_d needed for deep field weakening. This design trade-off creates a direct link between electromagnetic performance targets and material selection [14].

It is noted that SmCo has a much higher Curie temperature than Nd-Fe-B, resulting in greater magnetothermal stability at elevated temperatures. The bonded Nd-Fe-B magnet exhibits moderate magnetic strength with reduced coercivity due to its composite structure, while ferrite Y32 shows the lowest B_r and $H_{c,j}$, characteristic of a cost-effective but weak magnet. These curves establish the physical foundation for the comparative PMa-SynRM evaluation presented in this study.

V. PMa-SynRM Performance Evaluation Under Varying Permanent Magnets

The PMa-SynRM design was examined using four different magnets in Table II under various DC bus voltages ranging from 400 V to 800 V and peak current levels between 480 A and 650 A. Torque, output power, efficiency, and power factor are used to evaluate the motor performance of the PMa-SynRM

979-8-3315-8138-1

shown in Fig. 3 using ANSYS Motor-CAD. The maximum operating speed is set at 20,000 rpm.

TABLE II. PMa-SynRM Design and Operation Data Equipped with NdFeB.

Parameter	Data	Units
Peak Current	480	Amps
DC Bus Voltage	400	V
Permanent magnet flux	0.1103	Wb
Inductance in *q*-axis, L_q	0.3116	mH
Inductance in *d*-axis, L_d	0.187	mH
Stator copper resistance, R_s	0.09048	Ω
Inertia	0.031684	$kg{\cdot}m^2$
Pole pairs	4	
Output Power	86694	Watts
Maximum Torque	312.94	Nm
System Efficiency	94.255	%
Power Factor (Phasor)	0.93358	

Table II summarizes the key parameters of the tested PMa-SynRM (NdFeB example). The motor targets EV traction, with a 3000-rpm base speed, 20 000-rpm maximum speed, a 400-V DC bus, and a 480-A peak phase current. Its 0.09048-Ω stator resistance limits copper loss. The d- and q-axis inductances are 0.187mH and 0.3116mH, respectively. Under rated conditions, the machine produces about 86.7 kW with 94.26 % efficiency and a 0.93 power factor, confirming robust performance for EV applications.

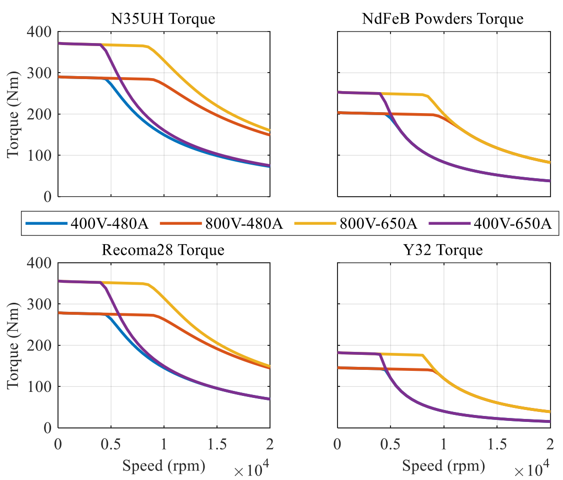

Fig. 5. Torque–speed comparison of evaluated magnets

The results of the simulated motor performance are shown in Figs. 5-6. From Figs. 5–6, the 800 V–650 A (yellow) voltage–current combination demonstrates clear advantages for all four magnet materials in terms of maximum torque, output power, and base speed. Despite their higher cost, both N35UH and Recoma 28 produce impressive torque and power levels in the designed PMa-SynRM motor. The additional magnet flux component, λ_m, and back-EMF discussed in Section II and III allow the motor to generate more torque when a stronger negative d-axis current is applied, as confirmed by the test results. The NdFeB powder and Y32 magnets show similar behavior to the rare-earth materials but at a moderate or lower performance level. These materials may be more suitable for other motor applications where the torque and magnetic field requirements are less demanding.

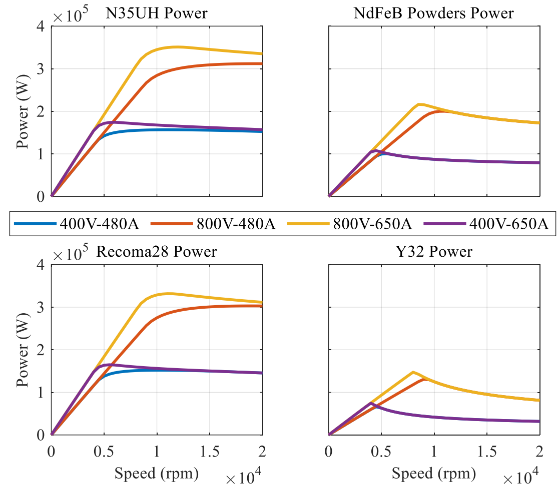

Fig. 6. Power–speed comparison of evaluated magnets

TABLE III. Performance of the simulated SynRM and PMa-SynRM at 3000RPM on 800V-650A.

Performance	SynRM	Ferrite	Bonded NdFeB	SmCo	NdFeB
Torque (Nm)	102.51	179.68	250.44	352.97	368.88
Power (kW)	32206	56.48	78.68	129.24	115.89
Power Factor	0.23	0.38	0.52	0.71	0.73
Efficiency	77.11	85.69	89.31	92.15	92.47

Tables III and IV summarize the SynRM and PMa-SynRM performance at 3000 rpm and 15 000 rpm under 800 V and 650 A. As expected, the pure SynRM delivers the lowest torque, power, and power factor due to the lack of PM excitation. Adding ferrite magnets produces a notable improvement, reaching 179.7 Nm at 3000 rpm and 60.6 Nm at 15 000 rpm, while raising the power factor 0.52 and efficiency to 93.2 %. This shows that even low-cost magnets can strengthen saliency and reduce current phase lag.

The NdFeB-assisted design offers the best overall performance, achieving up to 368.9 Nm and 219.8 Nm torque at low and high speed, respectively, with the highest power output and strong efficiency (>92 %). SmCo provides comparable high-speed capability with slightly lower performance, whereas bonded NdFeB yields mid-range performance suitable for cost-sensitive designs. Overall, ferrite offers a meaningful upgrade over a pure SynRM, while NdFeB remains the preferred choice when high torque density, efficiency, and wide flux-weakening range are required.

TABLE IV. Performance of the simulated SynRM and PMa-SynRM at 15000RPM on 800V-650A.

Performance	SynRM	Ferrite	bonded NdFeB	SmCo	NdFeB
Torque (Nm)	3.12	60.62	117.54	205.34	219.83
Power (kW)	4.91	95.22	184.65	322.54	345.30
Power Factor	0.26	0.52	0.69	0.83	0.85
Efficiency	74.32	93.18	95.07	95.42	95.49

However, the drawbacks of the high voltage–current combination of 800 V–650 A (yellow) start to appear in the power factor and efficiency, as shown in Figs. 7–8. The additional current introduces more thermal stress to the windings and stator, and the resulting temperature rise increases iron losses and weakens the magnetic field through partial demagnetization. N35UH and Recoma 28, which offer stronger

979-8-3315-8138-1

power performance, would require a reduction in voltage and current to maintain good efficiency. The relative thermal robustness of the assessed magnet materials can be inferred from their intrinsic coercivity and corresponding B–H characteristics. Detailed thermal impact study of the four different magnets is beyond the scope and page limit of this paper and will be reported in the future work.

The results also indicate that the DC bus voltage has a more significant influence on the power factor for the NdFeB powder and Y32 materials. In terms of relative performance trends shown in Figs. 7 and 8, the results also indicate that optimized PMa-SynRM designs using sintered NdFeB magnets can achieve torque density and efficiency comparable to those of documented IPM traction motors, while using less magnet volume and a simpler rotor topology. This suggests that PMa-SynRM machines can serve as a viable alternative for EVs when designed and operated under suitable conditions.

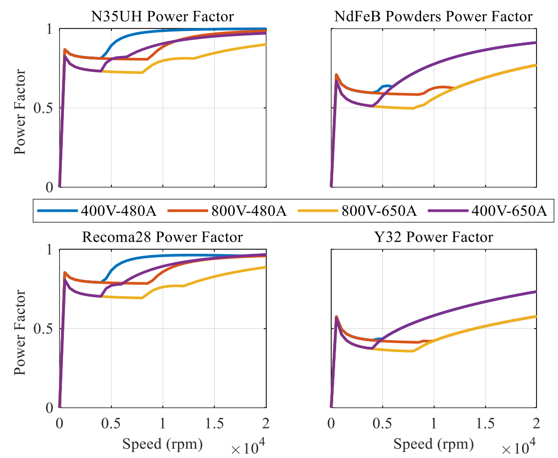

Fig. 7. PF–speed comparison of evaluated magnets

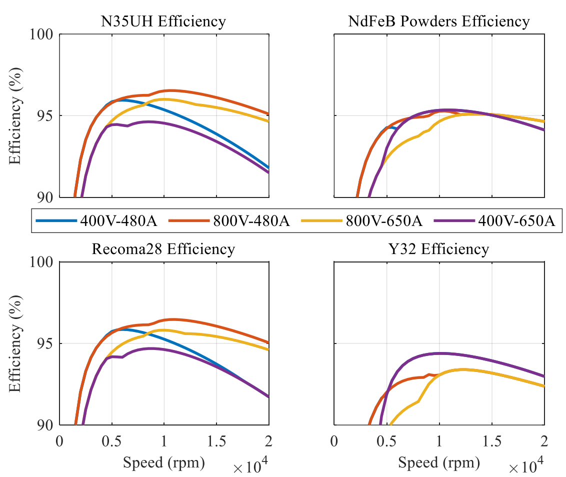

Fig. 8. Efficiency–speed comparison of evaluated magnets

VI. CONCLUSION

This study examined how four magnet types—NdFeB, SmCo, bonded NdFeB, and ferrite—affect PMa-SynRM performance for EV applications. NdFeB provides the highest torque, power, and power factor due to its strong remanence, though it is costly and less thermally robust. SmCo offers similar magnetic strength with superior high-temperature stability but at the highest material cost. Bonded NdFeB delivers moderate performance with simpler manufacturing and lower eddy-current losses. Ferrite has the weakest flux but excels in cost, stability, and rare-earth-free sustainability. Overall, magnet choice strongly depends on performance targets and budget: NdFeB and SmCo suit high-performance EV drives, while bonded NdFeB and ferrite support economical or moderate-power designs. These results demonstrate that magnet material selection alone can substantially reshape the operating envelope of PMa-SynRM traction motors, even under fixed geometry and inverter constraints, underscoring the importance of material-level design decisions in EV motor optimization.

ACKNOWLEDGMENT

This work was supported by the National Science Foundation under award No. RAISE-CET 2402634.

REFERENCES

[1] T. A. Huynh and M.-F. Hsieh, "Comparative study of permanent-magnet-assisted synchronous reluctance machine and interior permanent magnet synchronous machine on constant-power-speed-range for EV applications," *IEEE Trans. Magn*., vol. 53, no. 11, pp. 1–6, 2017.

[2] G. Du, G. Zhang, H. Li, and C. Hu, "Comprehensive comparative study on permanent-magnet-assisted synchronous reluctance motors and other types of motor," *Applied Sciences*, vol. 13, no. 14, p. 8557, 2023.

[3] Y. Wang, Y. Zhao, and Z. Zhang, "Comparative study of non-rare-earth and rare-earth permanent-magnet motors for electric-vehicle applications," *Energies*, vol. 15, no. 8, p. 2711, 2022.

[4] International Energy Agency (IEA), Global Critical Minerals Outlook 2024. Paris, France: IEA Publications, 2024. [Online]. Available: https://www.iea.org/reports/global-critical-minerals-outlook-2024

[5] P. Lazari, Permanent Magnet Assisted Synchronous Reluctance Machines (PMa-SynRM) Employing Rare-Earth-Free/Less Magnets, Ph.D. dissertation, Univ. of York, UK, 2018. [Online]. Available: https://etheses.whiterose.ac.uk/id/eprint/23502/

[6] A. Vagati, B. Boazzo, E. Armando, and P. Guglielmi, "Permanent-magnet minimization in PM-assisted synchronous reluctance motors for wide speed range," *IEEE Trans. Ind Appl*., vol. 49, no. 1, pp. 31–41, 2013.

[7] J.-C. Son, "Performance enhancement of the permanent-magnet-assisted synchronous reluctance motor for electric-vehicle applications," *J. Electrical Engineering & Technology*, vol. 17, no. 6, pp. 3275–3285, 2022.

[8] T. A. Huynh and M.-F. Hsieh, "Performance analysis of permanent magnet motors for electric vehicle (EV) traction considering driving cycles," *Energies*, vol. 11, no. 6, p. 1385, 2018.

[9] G. Artetxe, D. Caballero, B. Prieto, M. Martínez-Iturralde, and I. Elosegui, "Eliminating rare-earth permanent magnets on low-speed high-torque machines: A performance and cost comparison of synchronous reluctance machines, ferrite permanent magnet-synchronous reluctance machines and permanent magnet synchronous machines for a direct-drive elevator system," *IET Electr. Power Appl*., vol. 15, no. 3, pp. 370-378, Mar. 2021.

[10] Arnold Magnetic Technologies, "N35UH Sintered Neodymium-Iron-Boron Magnets," Product Data Sheet, Nov. 2017. Available: https://www.arnoldmagnetics.com/wp-content/uploads/2017/11/N35UH-151021.pdf

[11] Arnold Magnetic Technologies, "RECOMA® Samarium-Cobalt Magnets," Arnold Magnetic Technologies Product Data Sheet/Catalog, 2014. Available: https://www.arnoldmagnetics.com/wp-content/uploads/2017/10/Recoma-Combined-160301.pdf

[12] M. J. Herchenroeder et al., "High performance bonded neo-magnets using high density isotropic Nd-Fe-B powder," *AIP Conference Proceedings*, vol. 1334, pp. 682-689, 2011, doi: 10.1063/1.3565194.

[13] Eclipse Magnetics Ltd., "Ferrite Magnets / Ceramic Magnets Datasheet," Eclipse Magnetics, 2014. Available: https://www.eclipsemagnetics.com/site/assets/files/19602/ferrite_ceramic_datasheet.pdf

[14] L. Uršič and M. Nemec, "Permanent magnet synchronous machine demagnetisation prevention and torque estimation control considering rotor temperature," *IET Power Electronics*, vol. 12, no. 9, pp. 1295-1304, Jul. 2019.

979-8-3315-8138-1